HYDROLOGICAL PROCESSES
Hydrol. Process. **22**, 2829–2837 (2008)
Published online 20 March 2008 in Wiley InterScience
(www.interscience.wiley.com) DOI: 10.1002/hyp.7027

Peat hydraulic conductivity in cold regions and its relation to pore size and geometry

William L. Quinton,[1]* Masaki Hayashi[2] and Sean K. Carey[3]

[1] *Cold Regions Research Centre, Wilfrid Laurier University, Waterloo, N2L 3C5, Canada*
[2] *Department Geology and Geophysics, University of Calgary, Calgary, T2N 1N4, Canada*
[3] *Department Geography and Environmental Studies, Carleton University, Ottawa, K1S 5B6, Canada*

Abstract:

Subsurface flow through peat plays a critical role in the hydrology of organic-covered, permafrost terrains, which occupy a large part the continental arctic, sub-arctic, and boreal regions. Hillslope drainage in these terrains occurs predominantly through the active flow zone between the relatively impermeable frost table and the water table above it. The hydraulic conductivity profile within this zone controls the subsurface drainage of snowmelt and storm water. Peat hydraulic conductivity profiles were examined at three sites in north-western Canada, each representing a widely occurring organic-covered, permafrost terrain type. Three independent measures of saturated hydraulic conductivity were used—tracer tests, constant-head well-permeameter tests, and laboratory measurements of undisturbed samples. At all three sites, the conductivity profiles contained very high values (10–1000 m d^{-1}) within the top *ca* 0·1 m where the peat is only lightly decomposed, a large reduction with increasing depth below the ground surface in the transition zone, and relatively low values in a narrow range (0·5–5 m d^{-1}) below *ca* 0·2 m depth, where the peat is in an advanced state of decomposition. Digital image analysis of resin-impregnated peat samples showed that hydraulic conductivity is essentially controlled by pore hydraulic radius. The strong dependence of hydraulic conductivity on hydraulic radius implies that peat soils subjected to similar degrees of decomposition and compaction have a similar hydraulic conductivity regardless of the location. This explains the similarity of the depth-conductivity profiles among all three terrain types. Copyright © 2008 John Wiley & Sons, Ltd.

KEY WORDS hydraulic conductivity; permeability; subsurface run-off; organic soils; permafrost; image analysis; hydraulic radius

Received 5 June 2007; Accepted 5 February 2008

INTRODUCTION

Peat deposits cover extensive parts of northern North America and Eurasia, in a variety of types of organic-covered terrain that includes arctic and alpine tundra, taiga, and boreal and sub-boreal bogs, fens, and other peatlands. The peat of these terrains is often very similar with respect to many of its physical and hydraulic properties. For instance, in areas underlain by permafrost, the organic cover typically contains an upper, lightly decomposed layer, underlain by a darker layer in a more advanced state of decomposition, although the thickness of the layers is highly variable. Furthermore, the peat of many cold-regions site types is derived mainly from a similar suite of *Sphagnum* species, which produce peat with a common range of interparticle pore diameters under similar environmental conditions (Quinton and Gray, 2003). The size and connectivity of pores is a critical property that controls the flux and storage of water in the active layer.

The increasing degree of decomposition with depth below the ground surface results in a decrease in the size of particles and interparticle pores, and an increase in the amount of solid material per unit volume, with depth (Verry and Boelter, 1978; Quinton *et al*., 2000). The total porosity includes the volume fraction of the relatively large, interparticle pores that actively transmit water, referred to as the 'active porosity' (Hoag and Price, 1997); and the relatively small, closed, and dead-end pores formed by the remains of plant cells. Active porosity decreases from as high as ~0·8 near the ground surface to <0·5 near the bottom of the active layer (Quinton *et al*., 2000), while the total porosity decreases by a relatively small amount. This is presumably because the decomposition and compression of peat preferentially affects large, interparticle pores. With the reduction in active porosity, saturated hydraulic conductivity can decrease by orders of magnitude within half a metre or so below the ground surface (Hoag and Price, 1995; Beckwith *et al*., 2003).

Many organic-covered terrains also exhibit a similar hydraulic response to rainfall and snowmelt inputs. For instance, hillslopes mantled with peat typically experience little or no surface flow, due to the large water-holding capacity of organic soils and their high frozen and unfrozen infiltration rates, which far exceed the rate of input from snowmelt or rainfall. Instead, hillslope drainage occurs predominantly below the ground surface through the saturated flow zone, which during soil thawing is defined as the zone between the relatively impermeable frost table and the water table above

* Correspondence to: William L. Quinton, Cold Regions Research Centre, Wilfrid Laurier University, Waterloo, N2L 3C5, Canada.
E-mail: wquinton@wlu.ca

Copyright © 2008 John Wiley & Sons, Ltd.

it. Consequently the hydraulic conductivity profile is a very important factor controlling the rate of subsurface drainage of snowmelt and storm water from organic-covered hillslopes in permafrost terrains (Quinton *et al.*, 2000). Furthermore, the similarities with respect to peat properties and hydraulic response offer the possibility of developing a method of modelling the flux of water through peat which is physically-based, and therefore applicable to the wide range of organic-covered terrains.

Hydraulic conductivity, K [L T^{-1}], can be expressed as (Freeze and Cherry, 1979, p. 27)

$$K = k\rho g/\mu \quad (1)$$

where k [L^2] is the intrinsic permeability of the soil, ρ [M L^{-3}] is the density of water, μ [M L^{-1} T^{-1}] is the dynamic viscosity of water, and g ($= 9{\cdot}8$ m s^{-2}) is gravitational acceleration. Since ρ and μ are known for a given temperature, the challenge in hillslope run-off modelling lies in estimating the spatial distribution of permeability. It is well known that the permeability of individual pores is proportional to the square of pore diameter, and numerous formulae have been proposed to estimate permeability from pore diameter (e.g. Carrier, 2003).

Quinton *et al.* (2000), Equation (5) proposed an equa tion that relates permeability to geometric mean pore diameter, d_G [L], determined from microscopic image analysis of peat thin sections;

$$k = 2{d_G}^2/C \quad (2)$$

where C is a dimensionless coefficient. They found that when the saturated zone is confined within either the upper peat layer or the lower, more decomposed layer, C tended to reasonably constant values equal to $C = \sim 300$ and $C = \sim 14\,500$ respectively. Using these separate values of the fitting parameter C, Equation (2) produced a reasonable match with measured hydraulic conductivity in both layers. However, their analysis provides little insight into the effects of pore geometry on permeability, since it considered only the diameter of pores, and assumed that all active pores were circular in cross-section.

With recent advances in computerized image analysis, detailed information on microscopic pore geometry can be obtained from digital images with relative ease. This type of information has allowed some researchers to calculate specific surface area from spatial correlation functions of pores (Blair *et al.*, 1996; Schaap and Lebron, 2001) and use it with the semi-empirical Kozeny–Carman equation (Berryman and Blair, 1987). Others have obtained reasonably accurate estimates of permeability on purely theoretical grounds by using information on individual pores within a sample and integrating the conductance of individual pores (Schlueter *et al.*, 1997); or by treating them as a network of interconnected pores (Lock *et al.*, 2002). Most of these studies on permeability using image analyses were focussed on mineral soils or sandstones. If similar techniques are applicable to peat, it will greatly enhance our ability to understand the effects of pore size and geometry on permeability (and hydraulic conductivity), and hence strengthen our capability to model subsurface flow.

The objectives of this article are to: (1) examine the depth-hydraulic conductivity profiles of organic soils at multiple sites representing different environments; (2) investigate how hydraulic conductivity is controlled or affected by pore size and geometry; and (3) test the applicability of simple methods for estimating the hydraulic conductivity from measurements of pore geometry using microscopic image analysis.

STUDY SITES

Field studies were conducted at three locations in Canada, each representing a widely occurring organic-covered terrain type (Figure 1). Granger Creek is a sub-arctic, alpine catchment, located 15 km south of Whitehorse, Yukon. Scotty Creek is a wetland-dominated, high boreal catchment, located 50 km south of Fort Simpson, Northwest Territories. Siksik Creek is an arctic tundra basin located at the northern fringe of the forest-tundra transition (Bliss and Matveyeva, 1992), 55 km north of Inuvik, Northwest Territories. The coordinates and climate normals of the three sites are listed in Table I.

Permafrost is present at all three sites, and each site has a continuous organic cover, with the thickest accumulation at Scotty Creek (*ca* 3 m), followed by Siksik Creek (0·2–0·5 m), and then Granger Creek (0·2–0·35 m). At each site, the peat profiles typically contain a *ca* 0·2 m upper, lightly decomposed layer, underlain by a darker layer in a more advanced state of decomposition that extends to the bottom of the active

Figure 1. The location of Scotty Creek, Granger Creek, and Siksik Creek in northern Canada

Copyright © 2008 John Wiley & Sons, Ltd.

DOI: 10.1002/hyp

Table I. The coordinates of the three study sites, location of the nearest long-term climate station, and 1971–2000 normal monthly mean air temperature and mean annual precipitation (Environment Canada, 2007). * The Whitehorse precipitation may underestimate the precipitation at Granger by 25 to 35% (Pomeroy and Granger, 1999)

Site	Latitude, longitude	Climate station	Air temperature (°C)		Precip. (mm)
			January	July	
Granger Creek	60°31′N, 135°07′W	Whitehorse Airport	−17·7	14·1	267*
Scotty Creek	61°18′N, 121°18′W	Ft. Simpson Airport	−25·4	17·2	369
Siksik Creek	68°44′N, 133°28′W	Inuvik Airport	−27·6	14·2	248

layer at Scotty and Siksik, and to the top of the mineral soil at Granger. By late summer, the average frost table depth is approximately 0·6 m at Scotty and Granger, and 0·3 m at Siksik.

At each site *Sphagnum* provides the main peat-forming species. At Granger basin, the ground cover is composed of a continuous cover of *Sphagnum* moss and various herbs, including Labrador tea (*Ledum sp.*), sedges, grasses, and lichens. Some woody vegetation is present, including willow shrubs (*Salix sp.*), and a few scattered spruce (*Picea sp.*) trees. Willow and birch shrubs, 2–3m in height occupy much of the channel and riparian zones, and extend upslope but decrease in density and height. In the midslope region, the shrubs are 0·5–1m high and scattered, and at the upper slope, only occasional patches of short (<0·5 m) shrubs occur. A few scattered white spruce (*Picea glauca*) occur within the watershed, which is considered above treeline.

At Scotty Creek, the major peatland types include peat plateaus, flat bogs and channel fens (Quinton and Gray, 2003); however, this study focussed on the peat plateaus because of their importance to run-off generation (Quinton and Hayashi, 2005). Peat plateaus support a diverse vegetation community that includes four tree species (*Picea mariana, Larix laricina, Pinus contorta, Betula papyrifera*), fifteen shrub species (predominantly *Betula, Ledum, Kalmia* and *Salix*), sixteen species of lichen (predominantly *Cladina*), thirteen species of bryophytes (predominantly *Sphagnum*), in addition to species of vine, club moss, fungi, liverwort, sedges, grasses, aquatic plants, horsetails, and flowers.

At Siksik Creek, mineral-earth hummocks occur thro ughout the study basin and cover between 30 and 70% of hillslope surfaces. Their diameters range between 0·4 and 1·0 m, with crests rising 0·1–0·4 m above the surrounding interhummock surface. The hummock surfaces are bare or support a thin layer of lichen (*Alectoria* and *Cladina sp.*). The interhummock vegetation consists of sedges (*Eriophorum*) and surfaces are bare or support a thin layer of lichen (*Alectoria and Cladina sp.*). The interhummock vegetation consists of sedges (*Eriophorum* and *Carex sp.*) and small vascular plants (*Empetrum, Vaccinnium, Ledum,* and *Rubus sp.*) rooted in a continuous cover of moss (*Sphagnum sp.*).

METHODS

Tracer tests

Tracer tests were conducted at each study site to determine the horizontal hydraulic conductivity of the thawed portion of the saturated layer through which lateral subsurface drainage occurs. The results of the tracer tests for Siksik Creek and Granger Creek were reported by Quinton *et al.* (2000) and Quinton *et al.* (2004), respectively. The tracer tests at Scotty Creek were conducted using similar methods to those used at the other two sites, as described below. For each test approximately 80 l of 100 mg l^{-1} KCl solution was poured onto the ground surface of a peat plateau, along a 3–10 m application line that was oriented across the slope, and tracer concentration was monitored at several locations downslope of this line. In the test conducted on 17 September, 1999 and 20 June, 2000, tracer concentrations were monitored using chloride-sensing microelectrodes (Farrell *et al.*, 1991) connected to a Campbell Scientific 21X datalogger with readings made every 60 s and averaged and recorded every 15 min. In the tests conducted on 18 August, 2001 and 20 May, 2005, electrical conductivity sensors (YSI 3400) connected to a Campbell Scientific CR10X logger were used to monitor the concentration of total dissolved ions, which was dominated by KCl. The distance from the tracer application line to the sensors was 1–2 m in 1999 and 2000, 0·3–0·9 m in 2001, and 3·5 m in 2005. At each site, the tracer tests were repeated at different times during the development of the active layer in order to obtain estimates of the saturated hydraulic conductivity for different depths of the saturated zone within the peat profile.

Saturated hydraulic conductivity was computed from the Darcy equation:

$$K = v\phi_A/i \tag{3}$$

where ϕ_A is the active porosity of the peat estimated by image analysis of peat samples (below), v is the average velocity of flow through the active pores estimated by the tracer tests, and i is the magnitude of hydraulic gradient measured using a surveyor's level between the application line and each sensor location. The average pore velocity was computed as:

$$v = (L/t_c) \tag{4}$$

Copyright © 2008 John Wiley & Sons, Ltd.

DOI: 10.1002/hyp

where L is the straight-line distance between the tracer application line and the sensing electrode and t_c is the length of time between the time of application of the tracer and the time when the centre of mass of the tracer plume reached the sensor.

Guelph permeameter tests and laboratory conductivity measurements

Field-saturated hydraulic conductivity was measured using the constant-head well-permeameter method (Reynolds and Elrick, 2002) with a Mariotte system (Soil moisture Equipment Corporation, Guelph Permeameter). The measurements were taken on 26 August, 2001 at two locations on a peat plateau at Scotty Creek, within 10 m of the plot used for the tracer tests. At each location a 0·05-m diameter hole was hand-augered to the frost table, and water was poured into the hole to maintain the constant water-table position until the flow rate of water from the hole to the surrounding peat became steady, at which time the Guelph Permeameter was used to measure the flow rate (Hayashi and Quinton, 2004). Field-saturated hydraulic conductivity was calculated from the flow rate, the depth of water in the hole, and a parameter determined separately in the laboratory that represents the soil-water retention characteristics. An equation developed specifically for the interpretation of Guelph Permeameter data for soils underlain by an impermeable boundary, in this case the frost table, was used for calculation (Hayashi and Quinton, 2004), Equation (9). Since this method measures a depth-integrated hydraulic conductivity of the peat surrounding the auger hole between the water table and the frost table, the depth of measurement should be considered an interval rather than a point.

Peat samples were extracted from a 0·5-m deep soil pit at Scotty Creek by inserting high-density PVC sampling tubes (inner diameter = 0·15 m, length = 0·5 m) into the pit face at 0·09, 0·26, 0·29, and 0·37-m depths, following the approach of Quinton and Gray (2003). The samples were kept frozen until they were subjected to laboratory measurements of saturated hydraulic conductivity. From each core, one or two subsamples were cut into cubes having a volume of *ca* 216 cm^3 (= 6 cm × 6 cm × 6 cm^3). The four vertical sides of each cube were coated with a layer of urethane foam while the top and bottom were left uncoated. A total of six cubes was prepared, two each from the 0·09 to 0·37-m depth samples, and one each from the sample cores taken from the 0·26 to 0·29-m depths. For each cube, a constant hydraulic gradient was applied between the top and the bottom using the method described by Beckwith *et al.* (2003), and the horizontal hydraulic conductivity was calculated from the gradient and flow rate.

Peat sampling and image analysis

Peat was sampled from Scotty Creek and Granger Creek so that geometry of soil pores could be directly measured using image analysis software, following sample preparation in the laboratory. Field sampling involved inserting a high-density PVC sampling tube (inner diameter = 0·15 m, length = 0·5 m) vertically into the ground following the approach described in Quinton and Gray (2003). Three samples were taken each from the Scotty site and the Granger site. The Scotty sample cores filled the entire length of the sample tubes, and represent the upper 0·5 m of the peat accumulation; while for Granger, where the peat layer is much thinner, the sample tubes contained the entire peat accumulation, which for the three samples ranged between 0·2 and 0·3 m. At both sites, the samples were taken at distances of within 10 m of where the tracer tests were conducted, and most were sampled between the tracer application line and sensing points.

In the laboratory, all moisture was removed from the peat cores through the process of acetone replacement. The cores were then impregnated with fluorescent epoxy resin. Once the resin hardened, the cores were cut lengthwise in half. One cut face from each core was polished and photographed using a high resolution digital camera. During the imaging process, the cut face was exposed to two illuminations (normal and UV light), which enhanced the visual distinction between the pores and the rest of the image. Two sets of photographs for each subsample were taken under the two illuminations. Thirteen subsamples from the six cores were photographed and saved as colour digital images containing six million pixels. The images were imported to PCI Geomatica v10·0·4 Focus Module, where the red, green, and blue primary colour channels from the two illuminations were coregistered using the normal-light image as a base image. The data file for each sample was then classified over an area of 42·5 by 25·5 mm using an unsupervized fuzzy k-means algorithm (Mendenhall *et al.*, 1999). By utilizing two sets of optical data for each pixel, a six-dimensional consideration for class membership was accomplished. The classification generated sets of optimal, overlapping continuous classes that translate multiple attributes of each data point into k membership values in k classes or clusters (Arkin and Colton, 1956; Mendenhall *et al.*, 1999). It is recognized that the field and laboratory-based hydraulic conductivity measurements represented larger spatial scales than that represented by the thin sections for which hydraulic conductivity was computed.

To process the image further into binary classes of either void or solid space, the continuous classes were aggregated from deterministic visual comparison between the available imagery and hand-held inspection. The binary images contained 2500 by 1500 pixels, resulting in a pixel size (i.e. resolution) of 17 μm. The area and perimeter of all individual voids (i.e. pores) in the binary images were subsequently measured by the particle analyser function of the ImageJ v1·37 software. Figure 2 shows an example of the original image, shown in grey scale, and the classified binary image of a peat sample taken from the Granger site at a depth of 0·09 m.

Copyright © 2008 John Wiley & Sons, Ltd.

DOI: 10.1002/hyp

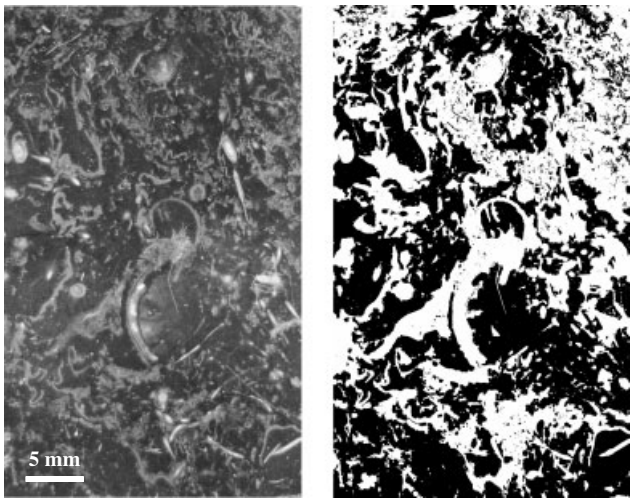

Figure 2. Grey-scale representation of the original image (a) of a peat block sampled at the Granger site from a depth of 0·09 m, and its processed binary image (b). Darker colours in the original image show the resin occupying pore spaces and lighter colours show the organic material. In the binary image, black areas represent pores

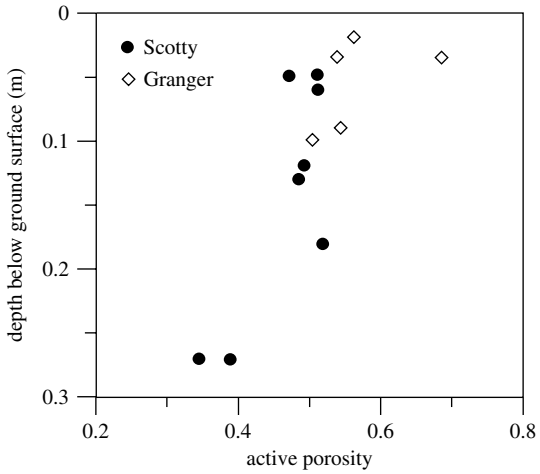

Figure 3. Active porosity of peat samples from the Scotty Creek and Granger Creek sites, estimated from the binary images of the samples

RESULTS AND DISCUSSION

Estimation of active porosity from image analysis

In estimating the active porosity from the binary images (e.g. Figure 2(b)), it was assumed that the pores too small to be resolved were predominately those of the inactive porosity—the closed and dead-end pores formed by the remains of plant cells, that contribute relatively little to flow (Hoag and Price, 1997). The minimum pore size depicted on the images was 1156 μm^2 (= 17 $\mu m \times 17$ $\mu m \times 4$), since groupings of less than four pixels were considered 'noise' and therefore neglected. Figure 3 indicates that the active porosity was generally higher in the upper 0·15 m (0·47–0·69) than lower in the profile (0·38–0·58). In comparison the total porosity at these sites was reported to be 0·8–0·95 in the upper 0·15 m and 0·75–0·9 in the lower parts (Quinton and Hayashi, 2005, Figure 2(c)). Therefore, active porosity is substantially lower than total porosity, implying the presence of small, inactive pores within the solid organic fragments. The average values of active porosity for the upper ($\phi_A = 0{\cdot}53$) and lower ($\phi_A = 0{\cdot}42$) layers were used in Equation (3) to calculate hydraulic conductivity from the tracer data (given below).

Relation between hydraulic conductivity and depth

At Scotty Creek, saturated hydraulic conductivity was highest near the surface, decreased by three orders of magnitude from 0·1 to 0·2 m, and remained nearly constant below 0·2-m depth (Figure 4(a)), which corresponds approximately with the interface between the lightly decomposed upper peat layer and the more heavily decomposed lower layer. This trend was consistent among all three methods of measurement. The Scotty Creek data are plotted with the tracer-test data from the other two sites in Figure 4(b). In this graph, the Granger Creek data are extracted from Quinton *et al.* (2004, Figure 6) using only those points representing the flow mostly within the peat layer, and the Siksik data are extracted from Quinton *et al.* (2000, Figure 5) using a few representative points from each depth and location. Despite a large scatter of points, the depth trend of hydraulic conductivity is consistent among all three sites with the values decreasing by orders of magnitude in a transition zone between 0·1 and 0·2 m. At the Siksik site, a total of 65 measurements were made at several depth zones, each depth zone containing seven to 28 points. Within each zone, sequential numbers were assigned to all sample points, and a random number generator was used to select approximately 30% of points from each zone.

Although there is a lack of data points in the upper 0·1 m at all sites (Figure 4(b)), the bulk density of peat

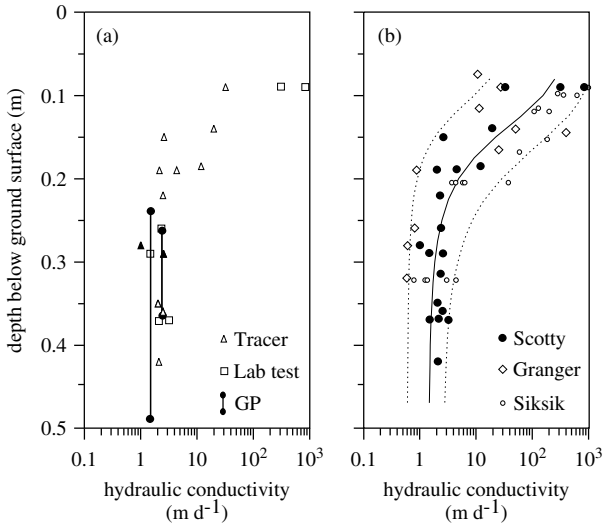

Figure 4. (a) Saturated hydraulic conductivity of peat at the Scotty Creek site. Symbols indicate the depth of sensors for tracer tests, the depth of samples for laboratory tests, and the interval measured by the GP method. (b) Compilation of peat hydraulic conductivity data from Scotty Creek (this study), Granger Creek (Quinton *et al.*, 2004), and Siksik Creek (Quinton *et al.*, 2000). The solid line indicates Equation (5) with the best-fit coefficients determined by the least-squares method (Table II), and the dashed lines indicate upper and lower envelopes of data points

Copyright © 2008 John Wiley & Sons, Ltd.

DOI: 10.1002/hyp

does not vary appreciably within the 0–0·1-m depth range, where the peat has a relatively uniform, lightly decomposed appearance (Quinton and Hayashi, 2005). Therefore, it is likely that hydraulic conductivity does not change substantially within the top 0·1 m. Most of the hydraulic conductivity reduction with depth occurs between 0·1 and 0·2 m at all sites (Figure 4(b)), even though the total thickness of the organic soil at Scotty Creek (>1 m) is much larger compared with that at the tundra sites of Siksik (0·2–0·5 m) and Granger (0·2–0·35 m). This suggests that the increase in peat thickness beyond 0·2 m has little effect on the overall range of hydraulic conductivity between the top and bottom of the peat profile. Therefore, it is reasonable to use a common equation to describe the variation in hydraulic conductivity with depth for all three sites.

To capture in a continuous function, the large hydraulic conductivity near the ground surface, its large reduction in the transition zone, and its low, asymptotic value in the bottom zone (Figure 4(b)), the following equation is proposed:

$$\log K(z) = \log K_{\text{btm}} + (\log K_{\text{top}} - \log K_{\text{btm}})/[1 + (z/z_{\text{trn}})^n] \quad (5)$$

where z [L] is depth below the ground surface, K_{top} and K_{btm} are the hydraulic conductivity [L T^{-1}] of the top and the bottom of the peat profile, z_{trn} [L] is the transition depth, and n is a dimensionless constant governing the shape of the transition curve. To assign the parameter values in Equation (5), it was assumed that the transition depth is the mid point between 0·1 and 0·2 m (i.e. $z_{\text{trn}} = 0{\cdot}15$ m) and the bottom hydraulic conductivity is given by $K_{\text{btm}} = 1{\cdot}4$ m d^{-1}. The values of K_{top} and n were determined by applying the least-squares method to all data points in Figure 4(b). The resulting curve generated by Equation (5) is shown as a solid line in Figure 4(b), with parameter values listed in Table II. Two other sets of values were assigned to represent the lower and higher envelopes of hydraulic conductivity, shown as dashed lines in Figure 4(b).

Two approaches to estimating hydraulic conductivity from image analysis

The large reduction of hydraulic conductivity with depth (Figure 4) is most likely governed by the reduction in active porosity (Figure 3) and the size of individual pores due to decomposition and compression of the organic matter. In the following, we will try to explain how hydraulic conductivity may be influenced by the pore size and geometry, measured from the digital images, (e.g. Figure 2) using two approaches. The first approach is based on the aggregate statistics, namely active porosity and specific perimeter, and the second approach calculates hydraulic conductivity by summing the hydraulic conductance of all individual pores.

Table II. Parameter values in Equation (5) for the best-fit line (solid line in Figure 4(b)) and lower and upper envelopes (dashed lines in Figure 4(b))

	K_{btm} (m d^{-1})	K_{top} (m d^{-1})	z_{trn} (m)	n
Best fit	1·4	360	0·15	4·3
Lower envelope	0·6	30	0·12	4·3
Upper envelope	2·5	1200	0·18	4·3

Hydraulic conductivity estimates from active porosity and specific perimeter

The first approach is based on the Kozeny–Carman equation as presented by Berryman and Blair (1987), Equation (1);

$$k = \frac{1}{cF}\frac{\phi^2}{s^2} \quad (6)$$

where c is a dimensionless shape factor, F is a formation factor representing the tortuosity effect, ϕ is porosity, and s [L^{-1}] is the specific surface area defined as the total surface area of pores per unit volume of the porous medium (Bear, 1972, p. 50). For flow through a pipe, the ratio ϕ/s is equal to the hydraulic radius, R [L], defined as the ratio between the area of cross-section, A [L^2] and wetted perimeter, P [L];

$$R = A/P \quad (7)$$

Therefore, ϕ/s can be regarded as an equivalent (or average) hydraulic radius of the exceedingly complex flow channels in the porous medium (Bear, 1972, p.165). Given the equivalence between ϕ/s and R, Equation (6) indicates that permeability is proportional to the second power of hydraulic radius, in a manner consistent with the well-known Hagan–Poisseuille formula for the steady flow through a single, straight circular tube (Bear, 1972, p.162).

To use Equation (6) with the image analysis data, we note that the specific surface area in three-dimensional porous media can be approximated by the specific perimeter p [L^{-1}] in two-dimensional cross sections, defined as the total perimeter of pores per unit cross-sectional area;

$$p = \sum_i P_i/A_{\text{img}} \quad (8)$$

where P_i [L] is the perimeter of the i-th pore in the image and A_{img} [L^2] is the total image area. We also note that active porosity ϕ_{A}, instead of total porosity, should be used to represent the flow in peat. It is given by;

$$\phi_A = \sum_i A_i/A_{\text{img}} \quad (9)$$

where A_i [L^2] is the area of the i-th pore in the image. Since the formation factor F in the Kozeny–Carman equation is commonly assumed inversely proportional to

Copyright © 2008 John Wiley & Sons, Ltd.

DOI: 10.1002/hyp

porosity (Berryman and Blair, 1987), Equations (15), (6) can be re-expressed as;

$$k = C_p \phi_A (\phi_A / p)^2 \quad (10)$$

where C_p is a dimensionless coefficient.

Permeability was computed from Equations (8)–(10) and converted to hydraulic conductivity through Equation (1) for the thirteen digital images, using C_p as a fitting parameter to match the computed values to the solid line in Figure 4(b) with the least-squares method. When a single value of C_p was used for all depths, it was impossible to obtain a reasonably good match for both the upper (<0·15 m) and lower layers. Therefore, Equation (10) was used with two separate values of C_p for the upper and lower layers, which resulted in a reasonable match (Figure 5(a)). The best-fit values of C_p were $1{\cdot}1 \times 10^{-2}$ in the upper layer and $1{\cdot}4 \times 10^{-3}$ in the lower layer. This is similar to the results of Quinton *et al.* (2000) in that the fitting parameter C in Equation (2) was greatly different in magnitude between the upper and lower layers. These results suggest that peat hydraulic conductivity is strongly influenced by active porosity and specific perimeter, but the two parameters may not be the most effective indicator of hydraulic conductivity.

Hydraulic conductivity estimates from individual pore conductance

To further investigate the relation between hydraulic conductivity and pore size, a second approach was taken to derive hydraulic conductivity from the conductance of individual pores. This analysis follows Schlueter *et al.* (1997) who used hydraulic radius (R_i, given below) and the Hagen–Poiseuille formula to calculate the hydraulic conductance, C_i [L^4] of individual pores;

$$C_i = A_i {R_i}^2 / 2 \quad (11)$$

where A_i is the cross-sectional area of the i-th pore in an image, R_i is its hydraulic radius defined by;

$$R_i = A_i / P_i \quad (12)$$

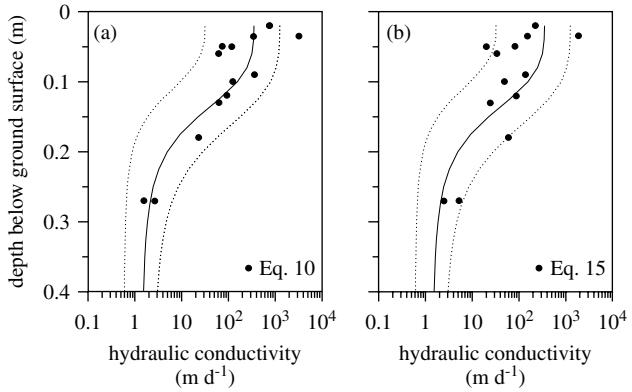

Figure 5. Saturated hydraulic conductivity computed for each of the thirteen images. This was done by computing the permeability using Equation (10) (a) and Equation (15) (b), and then converting the permeability values to hydraulic conductivity through Equation (1). Each symbol represents a single image. The lines indicate the hydraulic conductivity distribution modelled by Equation (5) (same as in Figure 4(b))

and P_i is its perimeter. It follows from Equations (11) and (12) that:

$$C_i = {A_i}^3 / (2{P_i}^2). \quad (13)$$

Schlueter *et al.* (1997) and Lock *et al.* (2002) showed that the hydraulic radius approximation Equations (11)–(13) gives reasonably accurate estimates of pore conductance with typical error values of 30% or less using numerical solutions of the Navier–Stokes equation in complex pore spaces. The total conductance, C [L^4], of all pores in the image is given by the sum of C_i divided by a dimensionless tortuosity factor, τ, and multiplied by the product of the dimensionless constriction factor f_c and stereological correction factor f_s (the meaning of which is described below):

$$C = \frac{f_c f_s}{\tau} \sum_i \frac{{A_i}^3}{2P_i^2}. \quad (14)$$

Finally, by definition, permeability [L^2] is the total conductance divided by A_{img};

$$k = \frac{f_c f_s}{\tau A_{img}} \sum_i \frac{{A_i}^3}{2P_i^2}. \quad (15)$$

The constriction factor accounts for the fact that the actual pore network consists of various-sized pores connected by 'bottle-necks' (i.e. constrictions), since Equation (13) treats individual pores as simple tubes having hydraulic radius of R_i. Lock *et al.* (2002), Equation (11) calculated theoretical constriction factors as a function of the ratio of minimum to maximum radius ($= r_{min}/r_{max}$) within a tube, using a saw-tooth model of pore tubes. The stereological factor corrects for the overestimation of the apparent area and perimeter of the individual pores resulting from the tendency that the two-dimensional sections cut across pores at oblique angles. Lock *et al.* (2002) showed that, for a circular pore tube, the stereological correction factor is given by $f_s = 3/8$. For the tortuosity factor, Schlueter *et al.* (1997) suggested $\tau = 3$ for hydraulically isotropic sandstone, whereas others (e.g. Blair *et al.*, 1996) used Archie's power law:

$$\tau \cong {\phi_A}^{-m} \quad (16)$$

where m is a dimensionless coefficient typically taking a value of 1·3–2·5 for most sedimentary rocks and close to 2 for sandstones (Mavko *et al.*, 1998, p. 283). To our knowledge, values of m for peat have not been reported in the literature.

Permeability was computed using Equation (15) for the thirteen images and converted to hydraulic conductivity through Equation (1). The constriction factor was estimated to be $f_c = 0{\cdot}03$ assuming $r_{min}/r_{max} = 0{\cdot}1$ in the saw-tooth model of Lock *et al.* (2002), and the stereological correction factor was assumed to be $f_s = 3/8$ (Lock *et al.*, 2002). Using Archie's exponent m as a fitting parameter to adjust the tortuosity term (τ) in Equation (15), a reasonably good match was achieved between the computed hydraulic conductivity and the

Copyright © 2008 John Wiley & Sons, Ltd.

DOI: 10.1002/hyp

solid line representing the overall trend of the field data (Figure 5(b)). The best-fit value of m was 2·3, which is within the reported range of 1·3–2·5 for sedimentary rocks.

The analysis indicates that peat hydraulic conductivity at the Scotty and Granger sites is essentially controlled by pore hydraulic radius. The strong dependence of permeability on hydraulic radius implies that peat soils subjected a similar degree of decomposition and compaction have a similar permeability regardless of the geographic setting. This explains the similarity of the depth profiles of hydraulic conductivity (Figure 4(b)) among all three sites. On the basis of this observation, empirical conductivity-depth relations such as Equation (5) may be applicable to a wide range of sites with minimum calibration of fitting parameters. Such equations will be useful for specifying peat hydraulic conductivity in large-scale hydrological models.

CONCLUSIONS

The saturated hydraulic conductivity of peat was measured at three study sites in northern Canada, representing widely occurring types of organic-covered, permafrost terrain. In all three sites, very high conductivity values (10–1000 m d^{-1}) were found in the top 0·1 m or so of the lightly decomposed peat layer, which dramatically decreased with depth to 0·5–5 m d^{-1} in the zone below 0·2 m. Despite the differences in site characteristics and the overall thickness of the peat accumulation, the conductivity-depth relation was represented by a single function applicable to all sites, suggesting that the function is potentially useful for a large-scale modelling of peat hydrology in cold regions. To investigate the effects of pore size and geometry on hydraulic conductivity, detailed pore geometry data with a resolution of 17 μm were obtained from digital image analysis of peat-sample cross-sections, and active porosity and specific perimeter were computed for each sample. Applying these data to a semi-empirical expression based on the Kozeny–Carman equation, a reasonably good match was obtained between the estimated and observed hydraulic conductivity. However, an empirical coefficient in the equation needed to be adjusted with depth by more than an order of magnitude to capture the dramatic change in hydraulic conductivity between the upper and lower layers. Using a more theoretical approach based on the hydraulic radius of individual pores, a good match was obtained between estimated and observed conductivity with a single set of parameter values. These analyses suggest that peat hydraulic conductivity is essentially controlled by pore hydraulic radius. The strong dependence of hydraulic conductivity on hydraulic radius implies that peat soils subjected similar degree of decomposition and compaction have similar conductivity regardless of locations. This explains the similarity of the depth profiles of hydraulic conductivity among all three sites.

ACKNOWLEDGEMENTS

The authors wish to dedicate this article to the late Professor Donald M. Gray, Division of Hydrology, University of Saskatchewan, whose thorough, rigorous style and thirst for new knowledge continues to inspire us. At Scotty Creek, we thank Gerry Wright and Roger Pilling of the Water Survey of Canada, and Nicole Wright. At Siksik Creek, the assistance of Dr. Philip Marsh and Cuyler Onclin of Environment Canada, and Joni Onclin and Brenda Sørensen is gratefully acknowledged. Ric Janowicz of Indian and Northern Affairs, and Newell Hedstrom and Dr. Raoul Granger of Environment Canada are thanked for their help at Granger Creek. We thank Tom Elliot and Dr. Richard Heck (University of Guelph, Land Resources Science) for their assistance with the analysis of soil images. Lindsay Meads and Michael Toews are also thanked for their assistance with laboratory measurements. We also gratefully acknowledge the support of the National Water Research Institute, the Natural Sciences and Engineering Research Council of Canada, the Canadian Foundation for Climate and Atmospheric Sciences, the Northern Scientific Training Programme (Indian and Northern Affairs Canada), and the Science Horizons Programme (Environment Canada).

REFERENCES

Arkin H, Colton RR. 1956. *Statistical Methods*. Barnes & Noble, Inc: New York.

Bear J. 1972. *Dynamics of Fluids in Porous Media*. Dover Publications: New York; 764.

Beckwith CW, Baird AJ, Heathwaite AL. 2003. Anisotropy and depth-related heterogeneity of hydraulic conductivity in a bog peat. I: laboratory measurements. *Hydrological Processes* **17**: 89–101.

Berryman JG, Blair SC. 1987. Kozeny-Carman relations and image processing methods for estimating Darcy's constant. *Journal of Applied Physics* **63**: 2221–2228.

Blair SC, Berge PA, Berryman JG. 1996. Using two-point correlation function to characterize microgeometry and estimate permeabilities of sandstones and porous glass. *Journal of Geophysical Research* **101**: 20359–20375.

Bliss LC, Matveyeva NV. 1992. Circumpolar arctic vegetation. In *Arctic Ecosystems in a Changing Climate: an Ecological Perspective*, Chapin III FS, Jefferies RL, Reynolds JF, Shaver GR, Svoboda J (eds). Academic Press: San Diego; 59–89.

Carrier WD. 2003. Goodbye, Hazen; hello, Kozeny-Carman. *Journal of Geotechnical and Geoenvironmental Engineering* **129**: 1054–1056.

Environment Canada. 2007. Canadian Climate Normals 1971–2000, accessed April 6, 2007 at http://www.climate.weatheroffice.ec.gc.ca/climate_normals/results_e.html.

Farrell RE, Swerhone GDW, van Kassel C. 1991. Construction and evaluation of reference electrode assembly for use in monitoring *in situ* soil redox potentials. *Communications in Soil Science and Plant Analysis* **22**: 1059–1068.

Freeze RA, Cherry JA. 1979. *Groundwater*. Prentice-Hall: Englewood Cliffs, NJ; 604.

Hayashi M, Quinton WL. 2004. A constant-head well permeameter method for measuring field-saturated hydraulic conductivity above an impermeable layer. *Canadian Journal of Soil Science* **84**: 255–264.

Hoag RS, Price JS. 1995. A field-scale, natural gradient solute transport experiment in peat at a Newfoundland blanket bog. *Journal of Hydrology* **172**: 171–184.

Hoag RS, Price JS. 1997. The effects of matrix diffusion on solute transport and retardation in undisturbed peat in laboratory columns. *Journal of Contaminant Hydrology* **28**: 193–205.

Lock PA, Jing X, Zimmerman RW, Schlueter EM. 2002. Predicting the permeability of sandstone from image analysis of pore structure. *Journal of Applied Physics* **92**: 6311–6319.

Copyright © 2008 John Wiley & Sons, Ltd.

DOI: 10.1002/hyp

Mavko G, Mukerji T, Dvorkin J. 1998. *The Rock Physics Handbook: Tool for Seismic Analysis in Porous Media*. Cambridge University Press: Cambridge, United Kingdom; 329.

Mendenhall W, Beaver RJ, Beaver BM. 1999. *Introduction to Probability and Statistics*. Duxbury Press: New York.

Pomeroy JW, Granger RJ. 1999. *Wolf Creek Research Basin: Hydrology, Ecology, Environment*. National Water Research Institute: Environment Canada; 160.

Quinton WL, Gray DM. 2003. Subsurface drainage from organic soils in permafrost terrain: the major factors to be represented in a runoff model. In *8th International Conference on Permafrost*, Phillips M, Springman SM, Arenson L (eds). A.A. Balkema Publishers: Zurich; 6.

Quinton WL, Hayashi M. 2005. The flow and storage of water in the wetland-dominated central Mackenzie river basin: Recent advances and future directions. In *Prediction in Ungauged Basins: Approaches for Canada's Cold Regions*, Spence C, Pomeroy JW, Pietroniro A (eds). Canadian Water Resources Association: Ottawa, Canada; 45–66.

Quinton WL, Gray DM, Marsh P. 2000. Subsurface drainage from hummock-covered hillslope in the Arctic tundra. *Journal of Hydrology* **237**: 113–125.

Quinton WL, Carey SK, Goeller NT. 2004. Snowmelt runoff from northern alpine tundra hillslopes: major processes and methods of simulation. *Hydrology and Earth System Sciences* **8**: 877–890.

Reynolds WD, Elrick DE. 2002. Constant head well permeameter (vadose zone). In *Methods of Soil Analysis, Part 4. Physical Methods*, *Soil Science Society of America Book Series 5*, Dane JH, Topp GC (eds). Madison: Wisconsin, WI; 844–858.

Schaap MG, Lebron I. 2001. Using microscope observations of thin sections to estimate soil permeability with the Kozeny-Carman equation. *Journal of Hydrology* **251**: 186–201.

Schlueter EM, Zimmerman RW, Witherspoon PA, Cook NGW. 1997. The fractal dimension of pores in sedimentary rocks and its influence on permeability. *Engineering Geology* **48**: 199–215.

Verry ES, Boelter DH. 1978. Peatland hydrology. In *Wetland Functions and Values: the State of Our Understanding, Proceedings of the National Symposium on Wetlands. Lake Buena Vista, Florida, November 7–10*, Greeson P (ed.). American Water Research Association: Minneapolis, MN; 389–402.

Copyright © 2008 John Wiley & Sons, Ltd.

DOI: 10.1002/hyp